Journal of Power Sources 195 (2010) 1529–1542

Contents lists available at ScienceDirect

Journal of Power Sources

journal homepage: www.elsevier.com/locate/jpowsour

Review

A review of recent progress in coatings, surface modifications and alloy developments for solid oxide fuel cell ferritic stainless steel interconnects

Nima Shaigan[a,*], Wei Qu[a], Douglas G. Ivey[b], Weixing Chen[b]

[a] Institute for Fuel Cell Innovation, National Research Council of Canada, Vancouver, British Colombia, Canada V6T 1W5
[b] Department of Chemical and Materials Engineering, University of Alberta, Edmonton, Alberta, Canada T6G 2V4

ARTICLE INFO

Article history:
Received 7 August 2009
Received in revised form
18 September 2009
Accepted 30 September 2009
Available online 9 October 2009

Keywords:
Solid oxide fuel cell
Interconnect
Stainless steel
Coating
Surface modification
Alloy development

ABSTRACT

Ferritic stainless steels have become the standard material for solid oxide fuel cell (SOFC) interconnect applications. The use of commercially available ferritic stainless steels, not specifically designed for interconnect application, however, presents serious issues leading to premature degradation of the fuel cell stack, particularly on the cathode side. These problems include rapidly increasing contact resistance and volatilization of Cr from the oxide scales, resulting in cathode chromium poisoning and cell malfunction. To overcome these issues, a variety of conductive/protective coatings, surface treatments and modifications as well as alloy development have been suggested and studied over the past several years. This paper critically reviews the attempts performed thus far to mitigate the issues associated with the use of ferritic stainless steels on the cathode side. Different approaches are categorized and summarized and examples for each case are provided. Finally, directions and recommendations for the future studies are presented.

Contents

1. Introduction

Progress in fabrication technology of SOFCs has enabled cell operation at lower temperatures without compromising the performance. At lower operating temperatures (e.g., 650–850 °C), metals can be practically utilized as interconnects and replace their traditional ceramic counterparts. Unlike ceramic processing, fabrication of complex-shaped metallic interconnects is feasible and inexpensive. In addition, metals exhibit excellent thermal and electrical conductivity in comparison with ceramics. Selecting the appropriate alloy satisfying interconnect criteria, however, presents challenges. Over the past few years, evaluation of different high-temperature alloys for interconnect application has been the subject of various studies [1–13]. Resistance to high-temperature oxidation and hot corrosion is the first requirement that a candidate alloy must meet, as the interconnect is required to serve at high temperatures in the presence of air and fuel. The alloy selected to serve as the interconnect is also required to show a low and constant area specific resistance (ASR). The generally accepted upper limit of ASR for SOFC interconnects is 0.1 $\Omega\,cm^2$ [1]. Furthermore, to avoid damage to the cell structure due to thermal cycles, the coefficient of thermal expansion (CTE) of the interconnect alloy

* Corresponding author. Tel.: +1 6042213000; fax: +1 6042213001.
E-mail address: nima.shaigan@nrc-cnrc.gc.ca (N. Shaigan).

0378-7753/$ – see front matter.
doi:10.1016/j.jpowsour.2009.09.069

must be compatible with that of the ceramic components (i.e., $\sim 10 \times 10^{-6}\,^{\circ}C^{-1}$ from 25 to 1000 °C). Chromia and alumina forming alloys are the only commercially used high-temperature oxidation resistant alloys. From an electrical conductivity perspective, only chromia forming alloys can be considered as candidates for interconnect application. Alumina forming alloys are, thus, excluded due to the insulating characteristic of the thermally grown, protective alumina layer. Chromia forming superalloys and austenitic stainless steels may not be suitable due to the high CTE of their austenitic matrix (i.e., $15–18 \times 10^{-6}\,^{\circ}C^{-1}$ from 25 to 1000 °C). Cr-based alloys with a body centred cubic (bcc) matrix meet the CTE match and electrical conductivity criteria. Nonetheless, they are expensive and not readily formable to complex structures. Ferritic stainless steels, hence, remain as the only candidate class of alloys due to their CTE match with ceramics, excellent formability and low cost. Nevertheless, commercially available ferritic stainless steels suffer from several shortcomings associated with their poor oxidation behaviour and oxide scale properties, especially on the cathode side which is exposed to air. Many research studies have focused on identifying and addressing the problems associated with oxidation of commercial ferritic stainless steels [14–25].

Oxidation of ferritic stainless steels, normally containing small levels of Mn, in air in the temperature range of 650–850 °C results in the growth of a double-layer oxide scale. This double-layer oxide scale consists of a protective chromia-rich subscale and an outer non-protective $(Mn,Cr)_3O_4$ spinel layer [25]. If the steel contains Si in amounts greater than ~0.5 wt.%, insulating, continuous or network-like films of silica can also grow under the chromia-rich scale [25].

The ASR of commercially available steel interconnects increases rapidly as the oxide scale grows [3]. There are several factors contributing to the increased resistance. The primary factor is the growth of the oxide scale. The conductivities of both $(Mn,Cr)_3O_4$ spinel and chromia are considerably smaller in comparison with the metallic substrate. An increase in the thickness of the oxide scale, therefore, proportionally increases the ASR. The formation of an insulating silica layer as the result of interfacial segregation of Si is another important factor which negatively affects the ASR of steels containing Si. There are also other contributions to increased ASR that are related to the metal/oxide scale interface. Interfacial imperfections, including voids and cavities as well as impurity segregation, reduce the scale-to-metal adhesion and actual surface area of intimate contact between the metal and oxide scale and, consequently, increase the interconnect ASR [16].

In addition to rapidly increasing ASR, the use of bare ferritic stainless steel interconnects is associated with another issue which is termed 'cathode Cr poisoning'. Under SOFC operating conditions, chromia-rich scales react with water or oxygen molecules and form volatile chromium oxyhydroxide ($Cr_2(OH)_2$) and/or Cr(IV) oxide (CrO_3). Volatile Cr species then migrate through the cathode, dissociate and deposit on the cathode/electrolyte interface as chromia and other unwanted compounds like $SrCrO_4$, in the presence of a lanthanum strontium manganite (LSM) cathode. The chromium deposition poisons the cathode's electrochemical activity and drastically deteriorates cell performance. The cathode Cr poisoning phenomenon has been the subject of many research studies [26–39].

Numerous coatings, surface treatments and alloy bulk composition modifications and developments have been considered as potential remedies in order to overcome the issues originating from the poor high-temperature oxidation and oxide scale properties of ferritic stainless steels, particularly for the oxidizing environment of the cathode side. This paper categorizes and reviews the recent advances in coating materials and technologies, surface treatments and alloy developments, for stainless steel interconnects, during the past several years. Most recent reviews are concerned with alloy selection and do not provide a thorough analysis of the current status of research on coatings and surface modifications.

2. Coatings for ferritic stainless steel SOFC interconnects

Various materials have been used in an effort to decrease oxide growth kinetics, increase oxide scale conductivity, improve oxide scale-to-metal adhesion and inhibit Cr migration from the chromia-rich subscales to the oxide surface. The materials used as coatings include reactive element oxides (REOs) [40–45], conductive perovskites [46–59], MAlCrYO (M represents a metal, e.g., Co, Mn and/or Ti) oxidation resistant systems [60–64], conductive spinels [65–81] and conductive, composite spinels [82–84]. The techniques used for coating of the mentioned materials on stainless steels include sol–gel techniques [41,45,48,49,56,67], chemical vapour deposition (CVD) [85,86], pulsed laser deposition [87], plasma spraying [50,52,88], screen printing and slurry coating, radio frequency (rf) magnetron sputtering [51,54,68,89,90], large area filtered arc deposition [60–62] and electrodeposition [65,71–74,79,81–84,91–94]. The following sections categorizes the coating materials and briefly introduces the techniques commonly used for deposition of such materials.

3. Reactive element oxide (REO) coatings

Ample experimental observations show that the addition of small amounts of reactive elements (e.g., Y, La, Ce, Hf, etc.) or their oxides in the form of dispersed particles effectively reduces the high-temperature oxidation rate and greatly improves oxide scale-to-metal adhesion for alumina and chromia formers [95–104]. The mechanisms through which reactive elements improve the oxidation resistance of high-temperature alloys are not yet fully understood. Various mechanisms have been suggested and reviewed in literature [97]. It has been shown that tramp impurities, especially S, in alloys tend to segregate to the metal–oxide scale interface and affect scale-to-metal adhesion [105]. Reactive elements form refractory, stable compounds with S and prevent its migration and interfacial segregation. Also, reactive element ions, which have a great affinity for oxygen, migrate through the scale grain boundaries to the surface where the activity of oxygen is the highest [99]. During their migration through oxide grain boundaries, relatively large reactive ions segregate at the oxide grain boundaries where they block the short circuit diffusion paths for migrating oxide forming cations (i.e., Cr). Inhibited outward migration of cations, then, prevents vacancy injection into the interface and nucleation of interfacial voids [99]. Coatings containing REOs can effectively improve oxide scale-to-metal adhesion and reduce oxide scale thickness, thereby decreasing the ASR of steel interconnects which is directly proportional to oxide thickness, oxide conductivity and the surface area of metal/oxide scale contact. Coatings with REOs are regarded as the first generation of protective coatings for steel interconnects.

The most popular techniques used for application of REO coatings include sol–gel and metal-organic chemical vapour deposition (MOCVD). Almost all REO films are thin (less than a micron) and can form perovskite chromites when reacting with diffusing Cr from the underlying scale.

In the sol–gel coating process, the substrate is immersed in a precursor containing salts, normally nitrates, of the elements to be deposited. The specimens covered with the precursor, are then dried to evaporate the excess solvent and heat treated to form surface oxides. The immersion can be repeated several times or performed with a controlled drag speed to adjust the final coating thickness.

Table 1
Nominal chemical composition (wt.%) of the steels discussed in the text.

Steel	Cr	Mn	Si	Al	Ni	Mo	La	Zr	Cu	Ti	Nb	C	S	P
AISI-SAE 430	16–18	1 max.	1 max.	–	–	–	–	–	–	–	–	0.12 max.	0.03 max.	0.04 max.
AISI-SAE 434	19	1 max.	1 max.	–	–	2	–	–	–	–	0.35	0.12 max.	0.03 max.	0.04 max.
AISI-SAE 446	23–27	1.5 max.	1 max.	–	–	–	–	–	–	–	–	0.2 max.	0.03 max.	0.04 max.
E-brite[a]	26–27.5	0.4 max.	0.4 max.	–	0.5 max.	0.75	–	–	0.2 max.	–	0.2 max.	0.01 max.	0.02 max.	0.02 max.
Crofer 22 APU[b]	20–24	0.3–0.8	0.5 max.	0.5 max.	–	–	0.04–0.2	–	0.5 max.	0.03–0.2	–	0.03 max.	0.02 max.	0.05 max.
AL453[a]	22.0	0.3	0.08	0.6	–	–	0.1	–	–	0.02	–	0.03 max.	0.03 max.	0.02 max.
ZMG232[c]	22.0	0.5	0.4	0.22	0.26	–	0.04	0.22	–	–	–	0.02	–	–
ZMG232L[c]	22.04	0.45	0.1	0.03	0.33	–	0.08	0.2	–	–	–	–	–	–
F18TNb[d]	17.8	0.5	0.5	–	–	–	–	–	–	0.3	0.4	0.02		
F17TNb[d]	17.5	0.5	0.5	–	–	–	–	–	–			0.02	–	–
IT-11[e]	26.4	–	0.01	0.02	–	–	–	–	–	–	–	0.009	–	–
Fe30Cr	29.95	–	–	–	–	–	–	–	–	–	–	0.0021	0.0009	–

The balance is Fe; steels may also contain trace amounts of N.
[a] A trade mark of Allegheny Ludlum.
[b] A trade mark of ThyssenKrupp.
[c] A trade mark of Hitachi Metals.
[d] A trade mark of Ugine Arcelor, Isbergues, France.
[e] A trade mark of Plansee AG, Reutte, Austria.

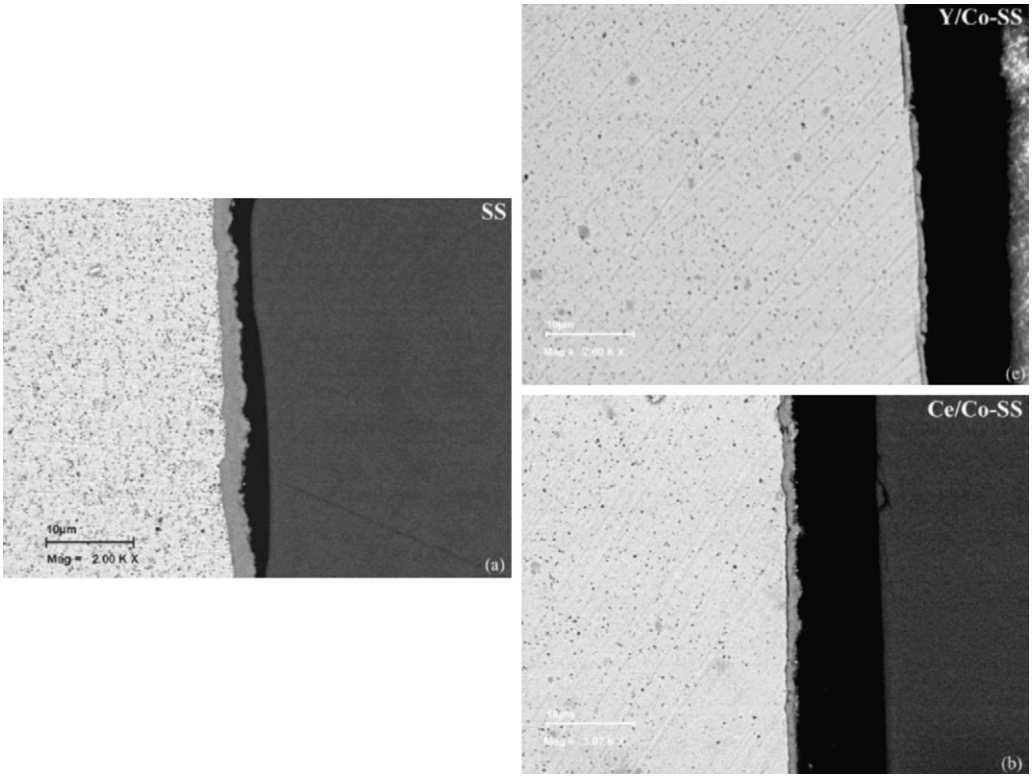

Fig. 1. Cross sectional backscattered electron (BSE) images of (a) uncoated, (b) Y/Co-coated and (c) Ce/Co-coated AISI-SAE 430 stainless steels oxidized for 1000 h. Courtesy Qu et al. [41] and Elsevier. Reprinted with permission.

Qu et al. [41] used two types of sol–gel coatings, Y/Co and Ce/Co, for AISI-SAE 430[1] stainless steel substrates with the purpose of reducing the oxidation rate of the steel and increasing the conductivity of the chromia-rich scales. Yttrium and Ce are reactive elements that can improve the oxide scale-to-metal adhesion and reduce the oxidation rate. Cobalt is regarded as a trivalent p-type dopant that can increase the conductivity of the chromia-rich scale. Fig. 1 shows cross sectional images of uncoated, Y/Co coated and Ce/Co coated specimens after oxidation at 750 °C in air for 1000 h. The oxide scale thickness using the Y/Co coating was less than 1 μm and that using the Ce/Co coating was between 1 and 1.5 μm. The uncoated samples had an oxide scale thickness of around 3 μm. It was found that Y accumulates mostly in the chromia-rich grain boundaries where it may inhibit Cr cation outward diffusion leading to slower oxidation kinetics. Cerium appears as ceria particles (Fig. 2a and b) at the chromia-rich (Fig. 2c)/$(Mn,Cr)_3O_4$ spinel (Fig. 2d) interface in Ce/Co coated, oxidized coupons. The ceria particles also acted as markers, and their presence at the boundary indicated that oxygen anions were the dominant diffusing species in chromia formation. In the absence of reactive elements, Cr outward diffusion is the predominant mechanism for oxidation. Cobalt was mostly distributed in the spinel phase in both cases.

The alternative technique for deposition of REO is the MOCVD process that was originally introduced by Eisentrant and coworkers [106–108]. In this process, volatile rare earth chelates (usually β-diketonates) are used as precursors. The precursor is

[1] For composition, see Table 1.

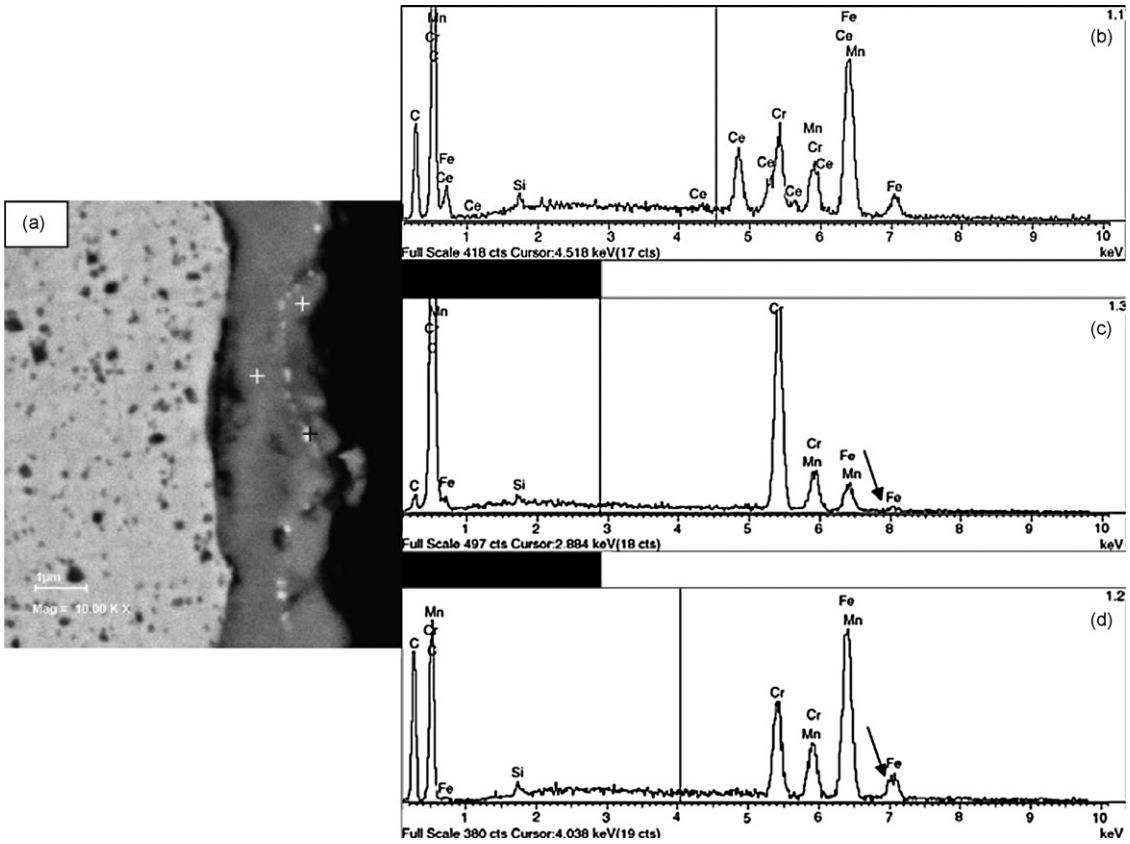

Fig. 2. (a) Cross sectional BSE image of Ce/Co-coated AISI-SAE 430 stainless steel oxidized for 1000 h. (b) Energy dispersive X-ray (EDX) spectrum from particles at interface between the two oxides. (c) EDX spectrum from inner oxide layer. (d) EDX spectrum from outer oxide layer. Courtesy Qu et al. [41] and Elsevier. Reprinted with permission.

heated to evaporation. The vapour along with carrier gases (N_2 and/or O_2) is then injected into a controlled atmosphere furnace, which heats the substrate. The precursor vapour then dissociates on the hot substrate surface and deposits a layer of reactive oxides. The byproduct gases are removed from the reaction chamber by the gas flow. This technique has been widely used in the semiconductor industry and to a lesser extent for SOFC applications [109–116].

Yttria coatings for Fe–30Cr[1] alloys (a laboratory made composition with negligible levels of S and C), applied by means of MOCVD, have been studied by Cabouro et al. [86]. The precursor used in the study was an organic compound of Y (tris-2,2,6,6-tetramethyl l-3,5 heptanedionato yttrium ($Y(tmhd)_3$)). The precursor was applied at 170 °C on the hot substrates (600 °C) while O_2 and N_2 were fed along with the precursor gas into the reactor. The coating thickness obtained with this technique was 100 nm. The short-term (24 h) oxidation tests at 800 °C showed that the application of Y_2O_3 via this technique significantly improves the oxidation resistance, refines the chromia scale grains and reduces the ASR. Spallation and cavity formation under the scale were also eliminated.

Coatings with REO can also be applied to form conductive perovskite layers. Fontana et al. [85] have studied coatings of La_2O_3, Y_2O_3 and Nd_2O_3 on Crofer 22 APU[1], AL453[1] and Haynes 230 (a Ni-base superalloy) substrates. The aim of this work was to form a conductive perovskite (chromite) layer via reaction between the coated binary oxides and Cr from the oxide scale. Among various combination of REO coatings and substrates, La_2O_3-coated Crofer 22 APU showed superior improvement particularly in terms of ASR. Other coating/substrate combinations also proved effective in reducing the oxidation rate and contact resistance, as well as elimination of oxide scale spallation.

Although coatings of REO have been shown to significantly enhance scale adhesion and reduce the oxidation rate and ASR, they are not suitable as Cr migration barriers. These coatings are normally thin (e.g., <0.2 μm) and porous and may not be effective at inhibiting Cr diffusion to the oxide surface and preventing Cr poisoning.

4. Rare earth perovskite coatings

Rare earth perovskites have the general formula of ABO_3 where A is a large trivalent rare earth cation (e.g., La or Y) and B is usually a trivalent transition metal cation (e.g., Cr, Ni, Fe, Co, Cu or Mn). Rare earth perovskites exhibit p-type electronic conduction in oxidizing environments and are stable in low oxygen partial pressures [2]. The electronic conductivity drops when the partial pressure of oxygen is low [2]. Low oxygen partial pressure leads to the formation of oxygen vacancies leaving electrons behind and, thus, the consumption of electron holes [2]. Large earth alkali cations with large ionic radii (e.g., Sr and Ca) can replace the rare earth cations on A sites. Also, perovskites can be doped with electron acceptors (e.g., Ni, Fe and Cu) at B sites. Doping can greatly increase the conductivity by up to two orders of magnitude [1]. Appropriate doping can also modify the CTE of conductive perovskites [1]. In addition to the advantages of being electronically conductive and exhibiting compatible CTE, rare earth perovskites can supply reactive elements (e.g., La) to the underlying, growing oxide scale and improve the oxidation behaviour. Application of these coatings may decrease the oxidation rate and improve scale adhesion and, thus, further reduce the ASR. However, perovskites are not suitable for protective purposes as they may transport oxygen ions.

The most commonly used perovskites for electronically conductive coating purposes are lanthanum strontium chromites (LSCr; $La_{1-x}Sr_xCrO_3$) [55,90], undoped lanthanum chromite (LCr; $LaCrO_3$) [51,54,56], lanthanum strontium manganites (LSM; $La_{1-x}Sr_xMnO_3$)

[50,57], lanthanum strontium cobaltites (LSC; $La_{1-x}Sr_xCoO_3$) [90] and lanthanum strontium ferrites (LSF; $La_{1-x}Sr_xFeO_3$) [59,70], even though other perovskites may give similar results. Perovskite coatings may be applied on stainless steel substrates by a variety of techniques including radio-frequency (rf) magnetron sputtering [51,54,57,68,89,90], sol–gel [56] and pulsed laser deposition [87].

The main technique used for deposition of perovskites on stainless steel is rf magnetron sputtering. In rf sputtering, insulating coatings are attainable due to the existence of a resonating circuit which couples the insulating electrode through an impedance and maintains the discharge [117]. An oscillating power source with a frequency higher than 50 Hz is required for rf sputtering [117]. The deposition rate can be increased if the rf and magnetron sputtering techniques are combined. In magnetron sputtering, a strong magnetic field above the target confines the ejected secondary electrons in the near-target region by changing the electron trajectories [117]. The energy of the trapped electrons in the near-target region enhances the ionization of the target and deposition rates [117]. Due to the ability of the technique to coat with ceramic materials, this method has been used for perovskite coatings. This method, however, is highly dependent on line-of-sight and both sides of the substrate cannot be coated at the same time.

Yang et al. [53] studied two types of perovskite coatings, including LSF and LSCr, for application as protective/conductive coatings for different grades of ferritic steel substrates including E-brite[1], Crofer 22 APU and AL453. The perovskite films were applied on the steel substrates via radio frequency (rf) magnetron sputtering. The coating thickness attained with this method was 3–4 μm. The coatings were not fully dense and contained porosity and cracks. Both coatings proved to be effective at reducing the ASR of the substrates for relatively short test periods (~250 h at 800 °C). Superior results were achieved with the application of LSCr relative to LSF coatings in terms of protection against oxidation and electrical properties. This was attributed to the lower ionic conductivity of LSCr and reduced oxygen anion inward transport giving better protection against oxidation. Among different substrates used in their study, E-brite exhibited the highest oxidation resistance with the application of coatings. These coatings, however, did not prevent oxidation of the substrate and the formation of a chromia-rich subscale. The ionic conductivity (for both O and Cr), porosity, cracking and non-protective nature of these films resulted in easy inward transport of oxygen and outward migration of Cr. Scanning electron microscope (SEM) cross sectional images of LSCr and LSF-coated and uncoated E-brite coupons after conductivity measurements at 800 °C in air for 200 h are shown in Fig. 3. Cracking and spallation of the coating from the substrate is clear in Fig. 3d.

Sol–gel coating methods have also been used for deposition of perovskites. Zhu et al. [56] used a sol–gel method to coat SAE-AISI 444 stainless steel substrates with LC and LSCr. The precursor contained nitrates of the elements in the coating and citric acid. The coated specimens were annealed at 800 °C in air for 1 h to achieve a crystalline perovskite structure. The coatings, however, were not dense and uniform after annealing. Both Sr-doped and undoped coatings noticeably decreased the oxidation rates at 800 °C and eliminated the scale spallation which occurred for uncoated steels identically oxidized. Coatings also effectively reduced the ASR. Doping with Sr unexpectedly did not show any effect on conductivity.

Multicomponent ceramics, including perovskites, can be deposited by pulse laser deposition techniques (PLD). Deposition in a PLD process is based on rapid evaporation of a solid target by means an incident, pulsating laser beam and deposition of the resulting vapour on a nearby, heated substrate [118]. The deposition is normally performed under controlled atmospheres or in vacuum. For oxide deposition, oxygen can be used as the background gas with a pressure smaller than 133 Pa. The process is simple and the composition of the deposited film and that of the target can be identical.

The application of PLD for interconnect coating has been reported by Mikkelsen et al. [87]. In their work, LSCr and $MnCr_2O_4$ spinel were used as the coating materials and Crofer 22 APU as the substrate. The coating thickness was adjusted to 0.5 μm. Oxidation tests performed at 900 °C for 500 h in humidified air showed

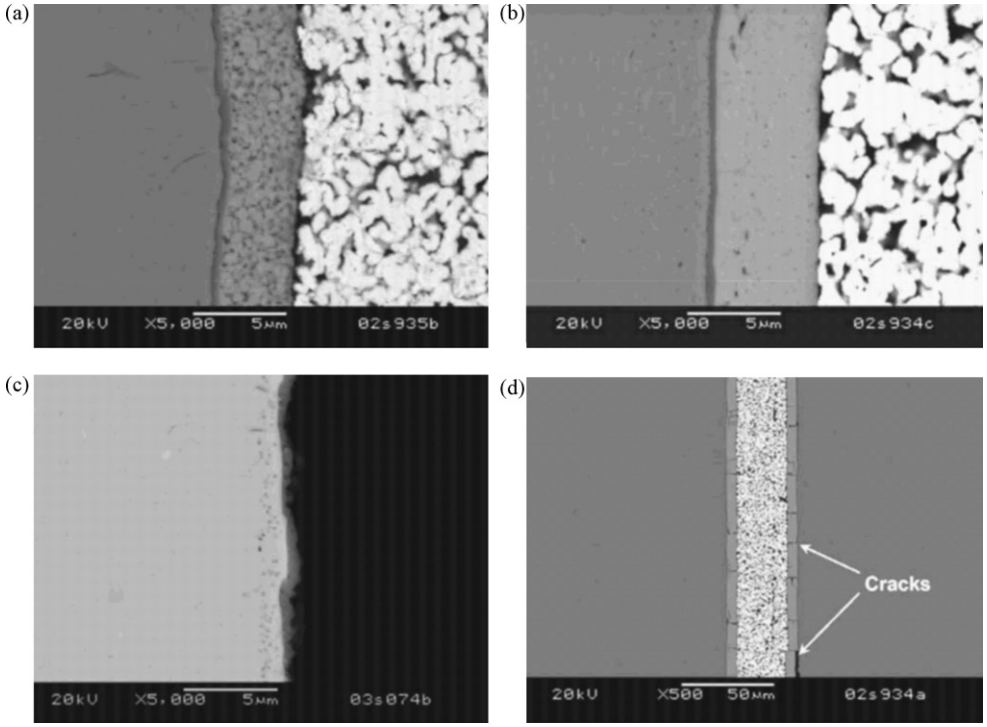

Fig. 3. SEM cross sectional images of (a) LSCr-coated E-brite, (b) LSF-coated E-brite, (c) E-brite and (d) low magnification of two LSF-coated E-brite samples with Pt paste in between. The images were obtained after 200 h of conductivity measurements. Courtesy Yang et al. [53] and the Electrochemical Society. Reprinted with permission.

Table 2
CTE and conductivity of spinels at 800 °C (Petric and Ling [120]).

	Mg	Mn	Co	Ni	Cu	Zn
Al	$MgAl_2O_4$	$MnAl_2O_4$	$CoAl_2O_4$	$NiAl_2O_4$	$CuAl_2O_4$	$ZnAl_2O_4$
σ[a]	10E–6	10E–3	10E–5	10E–4	0.05	10E–6
α[b]	9	7.9	8.7	8.1	–	8.7
Cr	$MgCr_2O_4$	$Mn_{1.2}Cr_{1.8}O_4$	$CoCr_2O_4$	$NiCr_2O_4$	$CuCr_2O_4$	$ZnCr_2O_4$
σ	0.02	0.02	7.4	0.73	0.4	0.01
α	7.2	6.8	7.5	7.3	–	7.1
Mn	$MgMn_2O_4$	Mn_3O_4	$CoMn_2O_4$	$NiMn_2O_4$[c]	$Cu_{1.3}Mn_{1.7}O_4$	$ZnMn_2O_4$
σ	0.97	0.1	6.4	1.4	225 (750 °C)	
α	8.7	8.8	7	8.5	12.2	
Fe	$MgFe_2O_4$	$MnFe_2O_4$	$CoFe_2O_4$	$NiFe_2O_4$	$CuFe_2O_4$	$ZnFe_2O_4$
σ	0.08	8.0	0.93	0.26	9.1	0.07
α	12.3	12.5	12.1	10.8	11.2	7.0
Co		$MnCo_2O_4$	Co_3O_4[d]			
σ		60	6.7			
α		9.7	9.3			

[a] σ is electrical conductivity ($S\,cm^{-1}$).
[b] α is CTE ($\times 10^{-6}\,°C^{-1}$).
[c] Decomposition at >700 °C.
[d] Decomposition at >900 °C.

that these coatings, in particular the LSCr coating, were able to reduce the growth rate of the underlying oxide scale. The capability for Cr retention and the electrical conductivities of these coatings, however, have not been examined.

Despite the limited improvements achieved with the application of perovskite films, such coatings do not substantially inhibit Cr migration or adsorb migrating Cr species resulting in Cr poisoning. This is attributed to the ionically conducting nature of the rare earth perovskites. These films are not successful oxygen barriers since they are oxygen diffusers to some extent and cannot be deposited in fully dense layers. Such coatings, however, have similar effects as REO coatings and improve oxidation resistance by supplying reactive ions to the underlying oxide scale.

5. Spinel coatings

Cubic spinel has the general formula of AB_2O_4 with A and B as divalent, trivalent and quadrivalent cations in octahedral and tetrahedral sites and oxygen anions on the face centred cubic (FCC) lattice sites. Spinel coatings have attracted significant attention recently. Depending on the choice of A and B cations and their ratio, spinels can be good electronic conductors and show excellent CTE match with the ferritic stainless substrate and other cell components, including the anode and cathode. Spinel coatings have shown excellent capability for absorbing Cr species that migrate from the chromia-rich scale to the scale surface and cause Cr poisoning. Research studies have been conducted to evaluate the suitability of different spinel compositions for application as potential conductive/protective coatings for stainless steel interconnects [119,120].

Electronic conductivity and CTE of various Cr containing spinel compositions, including $NiCr_2O_4$, $CoCr_2O_4$ and $MnCr_2O_4$ spinels, have been studied by Qu et al. [119]. Spinel powders in their study were synthesized from metal oxide powders by solid-state reaction followed by ball milling. The powders were then pressed and sintered at elevated temperatures to produce pellets and bars for electrical and microstructure examinations. All spinel systems tested showed similar CTE values, in the range of $7.2–7.6 \times 10^{-6}\,°C^{-1}$, that are close to that for chromia (CTE = $9.6 \times 10^{-6}\,°C^{-1}$) at 25–900 °C. It was also found that only $MnCr_2O_4$ and $NiCr_2O_4$ show lower electronic resistivities than chromia.

Petric and Ling [120] reviewed and studied the thermal and electrical properties of a vast variety of binary spinels containing Al, Mg, Cr, Mn, Fe, Co, Ni, Cu and Zn. These properties are listed in Table 2. It was found that spinels containing Fe exhibited the closest CTE values to ferritic stainless steels ($11 \times 10^{-6}\,°C^{-1}$). CTEs for other spinels evaluated were between 7 and $9 \times 10^{-6}\,°C^{-1}$ and the Cu–Mn and Co–Mn systems behaved anomalously. The highest conductivities were achieved with $MnCo_2O_4$ (60 $S\,cm^{-1}$ at 800 °C) and $Cu_{1.3}Mn_{1.7}O_4$ (225 $S\,cm^{-1}$ at 750 °C). The authors stated that $Mn_xCo_{3-x}O_4$, $Cu_xMn_{3-x}O_4$ ($1 < x < 1.5$), Co_3O_4 and $CuFe_2O_4$ are suitable candidates for the purpose of interconnect coatings, although there is no ideal composition.

Slurry coating methods including spraying [58,77] or screen printing [70,77] and plasma spraying [65,87] have been the main application techniques for spinel coatings in the past few years. Recently, electrodepositon of metals followed by heat-treatment/oxidation has been considered as a novel technique for spinel coating [65,71,73,74,79,81]. In addition, anodic electrodeposition of oxides from aqueous solutions containing the appropriate metal salts, followed by heat-treatment, has been reported as a method for spinel coating [72,91].

Slurries or pastes for spinel coating are made by mixing the spinel powders with an organic binder. A spinel powder with the desired properties is usually synthesized by high-temperature, solid state reactions between the oxides and/or carbonates of the spinel forming metals. A glycine-nitrate process [121] (known as GNP), followed by an optional milling process is an alternative way of producing uniformly distributed, fine spinel powders. In ceramic powder synthesis with GNP, glycine and metal nitrates of interest are dissolved in water to form an aqueous solution. The resultant precursor is then heated until the excess water evaporates leaving a viscous liquid behind. Further heating of this viscous liquid results in auto-ignition and production of a flame, heat, H_2O, CO_2, CO, N_2, NO_x and mixed metal oxide powders. GNP can yield fine (nano-scale), homogenous ceramic powders if the precursor stoichiometric ratios and reaction conditions are carefully adjusted. Dry milling is optionally subsequently utilized to further reduce the powder size and improve its homogeneity. GNP is widely employed for synthesizing ceramic powders used in fabricating SOFC materials including the cathode, anode and ceramic interconnect [52,122–134].

Yang et al. [75] have investigated a Mn–Co spinel coating with the nominal composition of $Mn_{1.5}Co_{1.5}O_4$ applied by means of screen printing on Crofer 22 APU substrates. The powder used for screen-printing was synthesized by solid-state reaction of Co_3O_4

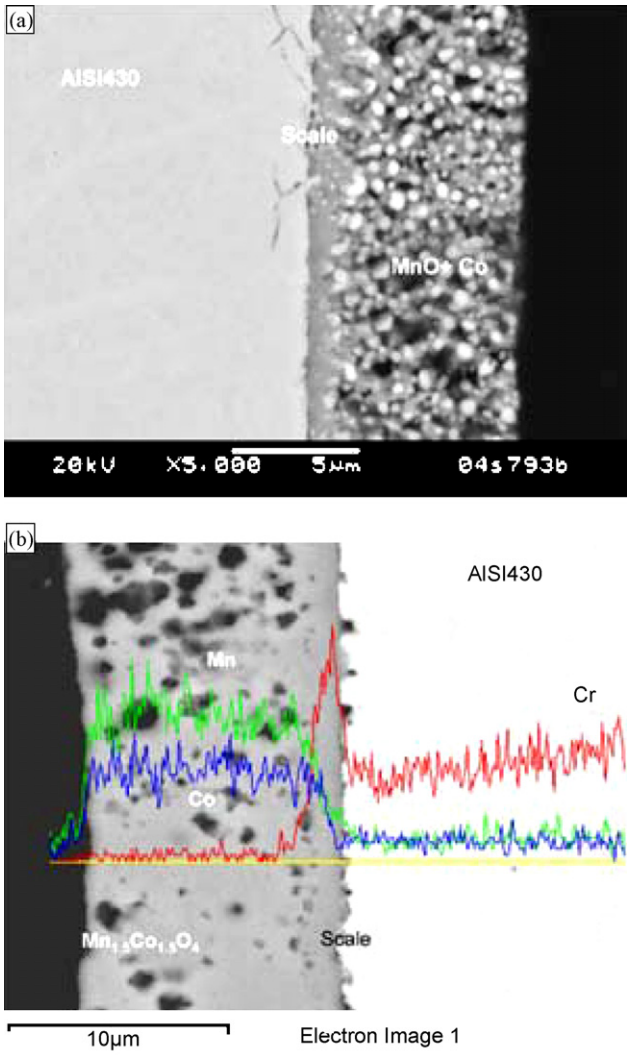

Fig. 4. SEM cross sectional images of protective layers on AISI-SAE 430 steel: (a) after annealing in Ar-2.75%H_2 at 800 °C for 24 h and (b) after oxidation in air at 800 °C for 100 h with superimposed EDX lines for Mn, Co and Cr. Courtesy Yang et al. [77] and the *International Journal of Hydrogen Energy*. Reprinted with permission.

and $MnCO_3$. The coating improved the electronic conductivity of the substrate and acted as an effective barrier against Cr migration. The ASR value for the spinel coated substrates was approximately 0.01 Ω cm^2 after 1000 h of oxidation in air at 800 °C, while the ASR value for uncoated substrates under identical conditions but after 400 h was 0.04 Ω cm^2. Yang et al., in another study [77], used two different methods of spinel powder preparation including solid-state reaction between Co_3O_4 and $MnCO_3$ and GNP. Powders prepared via GNP had finer and more homogenous particles which improved the coating density and performance compared to those synthesized by solid-state reaction. Spray and screen printing techniques were used to coat steel substrates such as Crofer 22 APU, E-Brite and AISI-SAE 430. Coated specimens were heat treated in a reducing atmosphere (i.e., Ar/3H_2O/4H_2) at 800 °C for at least 2 h. Annealing in air subsequently developed the spinel phase. This procedure was conducted to achieve high-density spinel coatings. Cross sectional SEM images of the reduced and oxidized coatings are shown in Fig. 4a and b, respectively. The image in Fig. 4b also has EDX line scans for Mn, Cr and Co superimposed on the image. In both reduced and oxidized conditions, a layer of Cr-rich oxide is present. According to the Cr line in Fig. 4b, no Cr concentration gradient is seen through the spinel layer. Upon heat treating in a reducing atmosphere, the Co content in the spinel was reduced resulting in the formation of metallic Co particles in an MnO matrix (Fig. 4a). Re-oxidation of this structure reformed the spinel and improved the density of the layer (Fig. 4b). Significant improvements in terms of contact resistance and oxidation protection were achieved for coated Crofer 22 APU and E-Brite substrates. After 400 h at 800 °C, the ASR values for coated Crofer 22 APU and E-brite were 0.013 and 0.007 Ω cm^2, respectively, while that for coated AISI-SAE 430 under identical conditions was 0.04 Ω cm^2 [77].

A $MnCo_{1.9}Fe_{0.1}O_4$ spinel coating for Crofer 22 APU, F18TNb[1], IT-11[1] and E-brite steel substrates was developed and studied by Montero et al. [69]. The specimens in their study were coated by screen-printing with $MnCo_{1.9}Fe_{0.1}O_4$ spinel paste. The coating thickness was approximately 60 μm. Reactive sintering was used for densification of the coated paste. This procedure included a reduction step, which was performed at 800 °C in a reducing, low oxygen partial pressure gas mixture consisting of Ar/3H_2O/4H_2. The reduction step was followed by an oxidation stage in air at 800 °C to reform the spinel. The authors pointed out that such a coating can effectively reduce the contact resistance between the cathode (LSF) and the steel. This coating also inhibited Cr outward diffusion and, thus, Cr poisoning. The presence of Mn in the alloy composition determined the effectiveness of the spinel coating. For Crofer 22 APU and F18TNb substrates, which contain small amounts of Mn, a decrease in ASR was noticeable, while the coating exhibited no significant improvement for IT-11 and E-brite, which contain negligible or trace amounts of Mn.

Plasma spray coating is an alternative technique to apply ceramic coatings with a thickness range of 0.05–0.5 mm on various substrate materials. The plasma torch consists of a water-cooled Cu anode and a W cathode [135]. The gas used for plasma generation is normally Ar or N_2 and H_2 or He. An oscillating voltage generates the arc and a direct current maintains it. Once plasma is produced, the coating powder can be fed into the torch where it melts and is accelerated in the plasma jet. Once the gas exits the nozzle, it expands and cools on the substrate resulting in rapid solidification of the injected coating material on the cold surface of the substrate [135]. With this technique, relatively thick coatings of high melting point ceramics can be deposited on metallic or ceramic substrates. However, due to rapid solidification and thermal stresses, cracks and internal porosity are common in the coating layers. The other limitation associated with this technique is that uniform coverage of the coating depends on the line-of-sight between the torch and substrate. As a result, coating of complex-shape interconnects is not practical via this technique. To achieve the desired layer properties, numerous parameters including torch design, powder size distribution, carrier gas and atmosphere must be carefully selected [135].

In Garcia-Vargas et al.'s [80] work, atmospheric plasma spraying (APS) of $MnCo_2O_4$ spinel followed by wet powder spraying of the same material was employed. APS produces a relatively dense, protective spinel layer while the wet powder spray forms a porous layer on the top of the relatively dense, protective layer. The purpose of the top porous spinel layer is to increase contact with the cathode and accommodate the stresses possibly caused by differences in CTE of the cell and interconnect. The substrate used in their work was F17TNb[1] ferritic stainless steel. A relatively low, stable ASR of 0.05 Ω cm^2 was obtained after 600 h of oxidation at 800 °C in air. The dense, protective spinel layer effectively reduced Cr outward migration.

Bonding of coatings to the substrates, the difficulty in synthesizing fine, homogenous spinel powders and coating porosity are issues when employing slurry and plasma spray techniques. Also, these coating techniques cannot be applied on complex-shape substrates due to the dependence on line-of-sight.

Recently, electrodeposition of metal layers or alloys followed by air annealing/oxidizing to form spinel layers directly on the steel substrates has been considered as an advantageous technique for spinel coating. The advantages of electrodeposition over slurry and plasma spray methods include better coating-to-substrate adhesion, denser, less porous spinel layers and good coverage of the electrodeposited coating on all substrate surfaces especially for complex-shaped interconnects. The thickness of the final spinel layer can be easily controlled by adjusting the deposition parameters (i.e., current density and time).

Electrodeposition refers to a process in which metal ions from an electrolyte are reduced and deposited on a conductive cathode substrate by application of an external electric current. The electrolyte is usually an aqueous solution containing simple or complex metal salts. Molten salt electrolytes can also be used when deposition from aqueous solutions is not possible (e.g., Al). The cathode surface must be conductive, clean and chemically active (free of native oxides and passivating layers) in order for a continuous, adherent coating layer to grow uniformly on the surface. The electrodeposition process continues as long as the external current source is connected to the anode and cathode and there is adequate metal ion supply in the electrolyte. Thus, coating thickness can range widely (from a few nanometers to hundreds of microns) using this technique.

In principle, spinel coating via electrodeposition is performed by plating a single layer or sequential layers of the desired transition metals (e.g., Mn, Co, Cu, Fe, Ni, etc.) or alloys on stainless steel substrates, followed by a subsequent heat treatment in air or some other oxidizing atmosphere. Annealing of the coated substrates in air results in simultaneous interdiffusion and oxidation of the electrodeposited metallic layers as well as elements from the substrate (i.e., Fe, Mn and Cr). Oxidation produces a well-adherent layer of spinel solid solution on the surface. A chromia-rich scale also grows under the thermally grown spinel layer. This spinel layer inevitably contains amounts of Fe, Mn and to lesser extent Cr as a result of diffusion from the substrate. The thickness of the spinel layer can be easily adjusted by changing the initial layer thickness and/or the oxidation/annealing conditions.

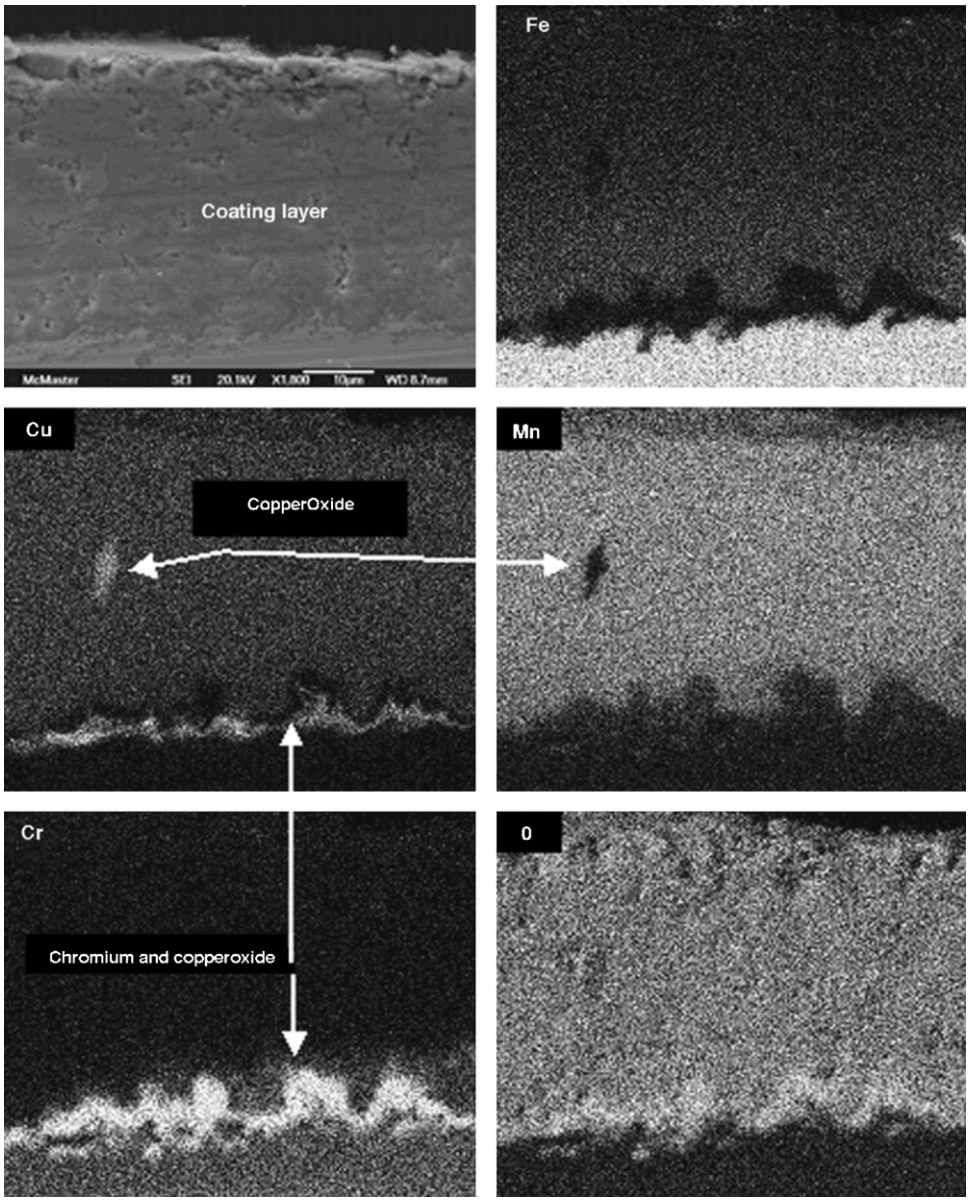

Fig. 5. Cross sectional SEM secondary electron (SE) image and EDX mapping of elements for $(Cu,Mn)_3O_4$ spinel obtained via electrodeposition, followed by annealing in air at 750 °C for 168 h. Courtesy Batenti et al. [65] and Elsevier. Reprinted with permission.

As mentioned previously, it has been found that $(Co,Mn)_3O_4$ and $(Cu,Mn)_3O_4$ spinels exhibit good conductivity and CTE match with ferritic substrates. Most research efforts have focused on these spinel systems for application as conductive/protective coatings. Wei et al. [71] were the first to develop and study $(Co,Mn)_3O_4$ and $(Cu,Mn)_3O_4$ spinel layers obtained by sequential electrodeposition of Mn and Co, as well as Cu and Mn, on AISI-SAE 430 stainless steel substrates. In their work, electroplating of Mn was conducted in a double compartment cell including a cathode compartment filled with Mn and ammonium sulphate as a catholyte (electrolyte in the cathode compartment) and an anode compartment using ammonium sulphate as an anolyte (electrolyte in the anode compartment). Glass frit tubes separated the two compartments. This was done to prevent formation and co-deposition of Mn hydroxide on the cathode. Cobalt chloride and sulphuric acid/copper sulphate plating baths were employed to deposit Co and Cu, respectively. Annealing of the coated steel was performed in argon for 2 h at 800 °C in order for interdiffusion of the sequentially deposited layers to occur. This also enhanced coating-to-substrate bonding. Oxidation tests and electronic conductivity measurements for the coated/annealed samples were done at 750 °C in air. It was shown that oxidizing of the sequentially plated metallic layers led to the formation of cubic spinel phases. The coatings obtained via this technique were shown to effectively protect the substrate and totally eliminate Cr outward diffusion. The ASR for both coatings was reported to be 0.003 Ω cm^2 at 750 °C after 1500 h of oxidation, which is markedly small compared to uncoated AISI-SAE 430 steel. In another study [65], the authors characterized the same $(Co,Mn)_3O_4$ and $(Cu,Mn)_3O_4$ spinel coatings in terms of microstructure. Fig. 5 shows an SEM image and corresponding energy dispersive X-ray (EDX) elemental maps for Fe, Cu, Mn, Cr and O for $(Cu,Mn)_3O_4$ spinel coatings oxidized for 7 days at 750 °C. Diffusion of Fe thorough the coating was observed while no Cr concentration gradient across the coating was seen, implying that Cr migration was inhibited. However, a relatively thick layer (~5–10 μm) of chromium-rich oxide formed under the spinel layer. Formation of this thick chromia-rich layer may have been due to interdiffusion of the coated metals into the substrate, which diluted the adjacent substrate surface in Cr. If the Cr content of the substrate is less than critical the Cr concentration threshold (i.e., 11 wt.%), the chromia layer will not be dense and pure enough to be protective. Localized breakdown of the thick, non-protective chromia-rich scales may happen at higher temperatures resulting in so-called breakaway oxidation and the formation of surface Fe-rich oxide nodules. The authors did not address this issue. The ASR, however, will not be adversely affected due to the high concentration of substrate elements (e.g., Fe and Mn) which can act as dopants in the chromia-rich scale and significantly increase the conductivity. The structure of the inner oxide layers was not identified by X-ray diffraction analysis (XRD) since the thermally grown oxide was too thick for sufficient X-ray penetration. In addition to the $(Cu,Mn)_3O_4$ spinel, copper oxides were present in the scale, depending on the Cu to Mn ratio in the as-deposited coating. Outward diffusion of Fe into the coating layers and inward diffusion of Co into the substrate were also detected. Both spinel coatings showed effective inhibition of outward Cr migration.

Composite spinel coatings can also be achieved by electrodeposition. Metal matrix composite deposits can be obtained by simply suspending the desired inert particles in the plating solution. Upon the application of an external current, metal-ion-covered, positively charged particles are attracted to the negative cathode and become adsorbed on the surface. The growth of the metal layer encapsulates the adsorbed particles in the matrix. Reactive element oxides, which can greatly improve the oxidation resistance and scale-to-metal adhesion, can be used as the secondary phase of the composite layer. Addition of reactive oxides also results in a dense, fine-grain and more protective spinel.

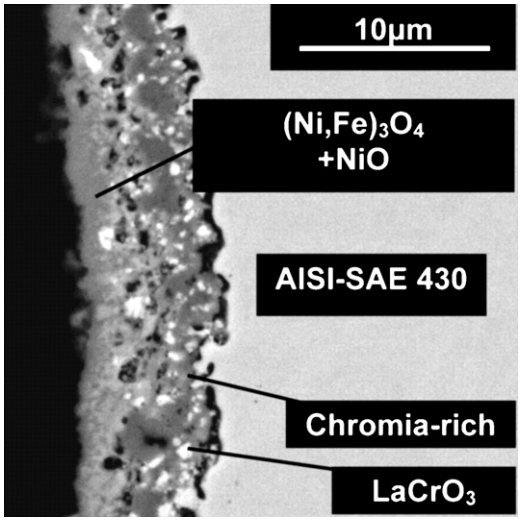

Fig. 6. Cross sectional BSE image of a Ni/$LaCrO_3$-coated AISI-SAE 430 coupon oxidized in air at 800 °C for 2040 h [83]. Courtesy Elsevier. Reprinted with permission.

Shaigan et al. [84] have developed, studied and optimized the co-deposition of lanthanum chromite ($LaCrO_3$) particles in a nickel matrix. It was found that by adjusting the deposition parameters, up to 35 vol.% of particles can co-deposit with Ni from a Watts Ni plating bath with a horizontally placed cathode. The oxidation behaviour and electrical conductivity of the Ni/$LaCrO_3$ composite coatings were studied in another paper by the same authors [83]. The coatings were applied to AISI-SAE 430 stainless steel substrates. It was observed that the scale was a double layer consisting of a particle filled chromia-rich subscale and an outer Ni/Fe-rich spinel together with NiO particles. The oxide structure after 2040 h of oxidation in air at 800 °C is shown in Fig. 6. A low, stable ASR (0.005 Ω cm^2 after 400 h) was achieved with the application of Ni/$LaCrO_3$ coatings. It was shown that in the absence of $LaCrO_3$ particles, Ni-plated steels exhibited breakaway type oxidation and hematite nodules started to appear after 600 h of oxidation in air at 800 °C. The main reason for breakaway oxidation was dilution of the substrate surface in Cr as a result of the inevitable inward diffusion of a portion of the coated metal into the substrate when exposed to high temperatures for oxidation.

In another study by Shaigan et al. [82], Ni was replaced with Co in the metal–matrix composite coating; Co-containing spinels have higher electronic conductivities. The coatings were also applied to SAE-AISI 430 stainless steel coupons. The Co/$LaCrO_3$ coating formed a triple-layer scale consisting of a chromia-rich subscale, a Co–Fe spinel mid-layer and a Co_3O_4 spinel top layer at 800 °C in air. This scale was protective, acted as an effective barrier against chromium migration into the outer oxide layer and exhibited a low, stable ASR of approximately 0.02 Ω cm^2 after 900 h at 800 °C in air. Coating with pure Co showed considerably higher specific weight gains in comparison with Co/$LaCrO_3$-coated, identically oxidized coupons. Also, after 1000 h oxidation at 800 °C in air, partial spallation of the scale (for Co-coated samples) was observed. Spallation occurred at the chromia–silica interface. No breakaway oxidation, however, occurred for Co-coated AISI-SAE 430 steels.

Alternatively, a mixture of metal oxides can be anodically electrodeposited onto steel surfaces from aqueous solutions containing metal salts and complexing agents. The as-deposited oxide layers are usually nano-crystalline or amorphous [91]. Subsequent heat treatment of the as-deposited oxides results in crystalliza-

tion and transformation of the mixed oxides to crystalline spinel structures [94,136]. In this method, the thickness of the coating is limited as the anode surface becomes covered with non-conducting oxides during anodic deposition. This procedure was developed by Wei et al. [91], who were the first to use anodic electrodeposition to form Co-rich $(Co,Mn)_3O_4$ spinel coatings on a ferritic stainless steel for the purpose of high-temperature oxidation protection. The electrolyte used in this work contained Co and Mn sulphates and ethylenediaminetetraacetic acid (EDTA) as the complexing agent. The cathode used was a Pt mesh. It was found that increasing the solution temperature to higher than 70 °C and the use of small current densities (~5 mA cm^{-2}) yielded crack-free oxide layers. Lower temperatures and higher current densities led to crack formation, the mechanism of which was not clear to the authors. The composition of the coating was easily controlled by adjusting the deposition temperature, the ratio of the metal salts in the electrolyte and current density. Increasing the solution temperature, the Co-to-Mn ratio in the solution and current density (up to 30 mA cm^{-2}) led to increased Co content in the deposits. The target Co-to-Mn ratio in the deposits was around 1:1 in order to achieve a more conductive spinel. The structure of the as-deposited oxide was a nano-crystalline, metastable and defective sodium chloride (NaCl)-type structure, which was independent of the deposition conditions and coating composition. Annealing of the as-deposited oxide-led to its transformation to FCC spinel or a distorted tetragonal spinel depending on the Co content of the oxide [94]. Co-rich oxides transformed to cubic spinel while their Mn-rich counterparts transformed to a tetragonal spinel structure [94]. The phase transformation happened at temperatures above 500 °C and is associated with reduction of Co and Mn cations to lower valences, migration of these cations from octahedral interstices to tetrahedral ones and the loss of oxygen [94]. In other work, Wei et al. [72] studied the protective and electrical properties of Co–Mn spinel coatings obtained by anodic electrodeposition. Two types of atmospheres were used to transform the as-deposited, defective NaCl structure to the cubic spinel structure. The environments selected for this purpose included air and forming gas (5%H_2–N_2), both at 800 °C for 10 h. Annealing in a reducing atmosphere led to the formation of a structure consisting of small metallic Co particles in an Mn_3O_4 matrix. A very thin layer of chromia and Si-rich oxide also formed beneath the coating. Pre-treating in air, however, resulted in spallation and formation of micro-cracks in the coating. Chromium from the substrate and the chromia-rich subscale diffused through the air pre-treated coating and formed a spinel solution layer containing Mn, Co and Cr. It was also found that only coatings pre-treated in forming gas showed protective properties, good adhesion to the substrate and an effectiveness in reducing the ASR values relative to the uncoated substrates.

6. MAlCrYO coatings

MAlCrY refers to a group of alloys that are almost exclusively used as high-temperature oxidation resistant coatings for gas turbine and jet engine blades working at temperatures above 1000 °C. These coating materials are alumina formers and, as such, would generally not be considered suitable for interconnect applications. Coatings with MAlCrY oxides (i.e., MAlCrYO), however, have been reported in literature for interconnect applications [60–64]. It has been shown that if the coating is thin (<5 μm) and Mn and/or Co is used as a part of the coating composition, a relatively low ASR (0.02–0.03 Ω cm^2) can be achieved [64]. The low ASR has been attributed to incorporation of Mn (from the coating and/or the substrate) into the oxide and the formation of spinel phases with Al, Cr, Co and Mn. These coating are effective in reducing Cr release from the surface.

Table 3
Comparison of different coating materials in terms of capability of improving electronic conductivity, Cr migration inhibition and oxidation rate reduction as well as simplicity of the coating process.

Coating material	Electronic conductivity	Cr migration inhibition	Oxidation rate reduction	Simplicity of deposition
REOs	Fair	Poor	Good	Good
Perovskites	Good	Fair	Poor	Fair
Spinels	Good	Good	Fair	Good
Composite spinels	Good	Good	Good	Good
MCrAlYO	Highly depends on composition	Good	Good	Poor

The technique used for the deposition of MAlCrYO coatings in Gannon et al.'s work [64] is large area filtered arc physical vapour deposition (LAFAD). In this process, the transfer of coating material from the target (cathode) occurs by a highly ionized metal plasma originating from the cathode arc spot under vacuum. The main disadvantage of this method is the deposition of particulates on the surfaces to be coated. This drawback has been overcome by the addition of magnetic coils which deflect the plasma. The deflected plasma passes through a series of baffles where droplets are captured [137]. This process is termed filtered arc deposition.

Table 3 compares the capability of different coating materials for reducing the contact resistance, Cr migration and oxidation rate of ferritic stainless steel interconnects as well as simplicity of the deposition processes. In summary, spinel coatings are the only coatings which exhibit good Cr retention, thereby inhibiting Cr poisoning. Also, spinel layers protect the underlying metal against oxidation to some extent and decrease and stabilize the ASR. The addition of reactive oxides greatly enhances the protective ability of the spinel layers. Coating with spinels does not require sophisticated instruments and can be performed easily by spraying, screen printing and electrodeposition techniques.

Table 4 summarizes the advantages and disadvantages of each coating technique discussed in the text. Electrodeposition for spinel coating, in comparison with other direct application techniques, is a simple technique which can be applied to coat complex configurations. Dense, uniform and adherent metallic layers can be deposited on the steel substrate to form thermally grown, protective/conductive spinel layers upon oxidation. The disadvantages of electrodeposition include the difficulty in depositing Mn and interdiffusion issues which may result in breakaway oxidation. Electrodeposition of Mn and its alloys presents challenges due to the large negative electrode potential of Mn in aqueous solutions as well as the brittle nature of metallic Mn [138]. Although Mn can be electrodeposited at high current densities, the deposits are readily soluble in the electrolytes [138]. Breakaway oxidation can be inhibited by the addition of REOs to the metallic coatings. Reactive element oxides are embedded in the protective scale and can greatly reduce the oxidation rate.

7. Surface treatments/modifications

Mechanical, thermal, thermo-mechanical, electrochemical and chemical surface treatments can profoundly affect the oxidation kinetics and oxide scale properties of high-temperature alloys. Mechanical surface deformation (cold work) increases the number of defects, particularly dislocations, in the alloy surface region. The defects provide rapid diffusion pathways for Cr to diffuse out, reach the surface and form a protective scale more rapidly and uniformly [139]. During the initial stages of oxidation, the abundance of such fast diffusion paths leads to accelerated nucleation and lateral growth of chromia to form a continuous, protective layer [139]. Since the temperature at which an interconnect alloy must oper-

Table 4
Advantages and disadvantages of different coating techniques discussed in the text.

Coating method	Advantage	Disadvantage
Sol–gel	• Simple • Applicable to ceramic coatings	• Thin, non-uniform coatings
MOCVD rf magnetron sputtering	• Applicable to ceramic coatings • Applicable to ceramic coatings	• Thin, non-uniform coatings • High cost • Dependent on line-of-sight • Cracked, porous coatings
PLD	• Applicable to ceramic coatings	• High cost • Dependent on line-of-sight
Slurry coatings	• Simple	• Non-uniform, porous coatings
Screen printing Plasma spraying	• Simple • Thick ceramic coatings possible	• Non-uniform, porous coatings • Porous coatings • Dependent on line-of-sight
Electrodeposition	• Simple • Applicable to complex shapes	• Difficulty for Mn deposition • Interdiffusion with substrate during oxidation leading to breakaway oxidation
Composite electrodeposition	• Simple • Applicable to complex shapes • REOs can be embedded into protective scale	• Difficulty for Mn deposition
Anodic deposition	• Simple • Applicable to complex shapes	• Limited coating thickness • Poor adhesion
LAFAD	• Applicable to ceramic coatings	• High cost • Dependent on line-of-sight

ate is higher than the recrystallization temperature, after formation of the protective oxide film, the deformed surface grains undergo recrystallization resulting in a higher number of grain boundaries. These grain boundaries further supply the oxide forming element from the bulk to the surface region of the alloy and prevent the dilution of the surface in Cr [25]. Therefore, it is expected that upon surface deformation, a more protective, denser scale will grow on the alloy surface.

Cooper et al. [25] studied the effect of sandblasting and cold rolling on oxidation kinetics of three different types of ferritic stainless steels including AISI-SAE 430/434[1] and Hitachi ZMG232[1]. The authors found that deformation increased the parabolic rate constant for oxidation of all three steels. Also, the proportion of spinel-to-chromia decreased or remained unchanged with surface deformation. No information, however, on the effect of surface deformation on electrical properties and scale-to-metal adhesion, which are directly affected by surface deformation, was reported.

Belogolovsky et al. [140] have studied the effect of various surface treatments on chromia scale adhesion for AISI-SAE 430 steels. The surface treatments included polishing with 240 and 600 grit sandpapers, electropolishing in phosphoric/sulphuric acid solution, pickling in hydrofluoric/nitric acid, sand blasting, heat-treating in a reducing atmosphere and applying Y nitrate coatings on both reduced and untreated samples. Grinding and sandblasting induce surface deformation which, in turn, provides diffusion paths for Cr during oxide growth by the formation of dislocations, other defects and new grain boundaries. These defects may assist the rapid formation of a protective oxide scale. Electrochemical polishing provides a smooth and even surface and acid pickling may remove surface contamination such as oxides. Heat treatment in a reducing atmosphere removes impurities such as S leading to the formation of a relatively pure, thin chromia protective scale. Belogolovsky et al. measured the oxide scale-to-metal adhesion via tensile pull testing for both treated and untreated samples which were oxidized in air at 800 °C for 458 h and cooled rapidly to room temperature. The results of the pull tests are shown in Fig. 7. The lowest force required for failure was for the sample ground with 600 grit sandpaper. Images from the spalled area (not shown here) indicated that voids formed along the polishing marks. The samples ground with rougher sandpaper (240 grit) showed higher resistance to pull testing. This was attributed to a smaller density of polishing marks which can increase void initiation during oxidation. Surface treatment using 240 grit sandpaper still decreased

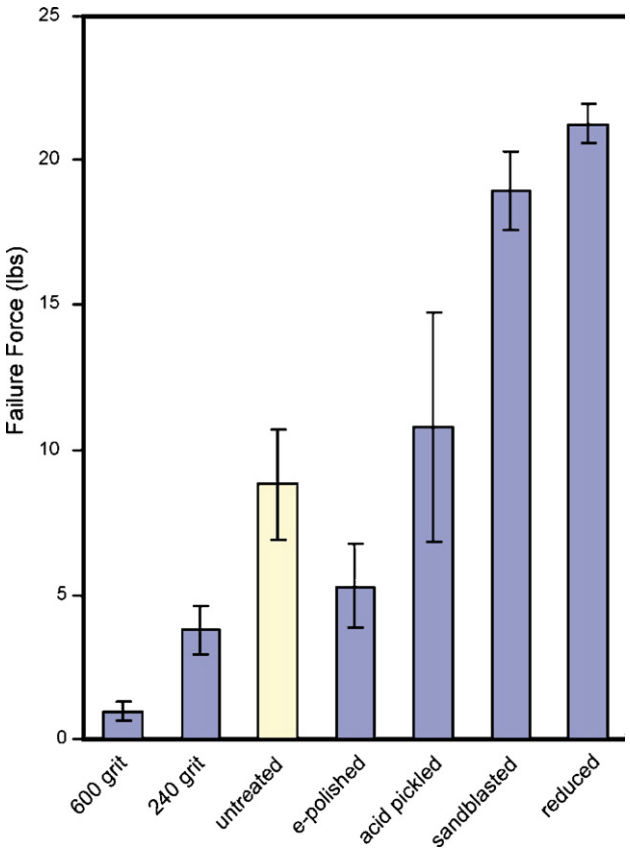

Fig. 7. The effect of different surface treatments on scale adhesion for AISI-SAE 430 samples treated and oxidized at 800 °C in air for 458 h. Courtesy Belogolovsky et al. [140] and Elsevier. Reprinted with permission.

adhesion of the scale in comparison with untreated samples. It was observed that the samples treated with electrochemical polishing developed voids at the metal surface grain boundaries. Acid pickling, however, did not change the force needed for failure. Sandblasting and heat-treating in a reducing atmosphere showed the greatest improvement in terms of scale adhesion. The improvement achieved with sandblasting was attributed to the difficulty for crack propagation along the interface as a result of a tortuous alloy surface shape. Heat-treating in reducing atmospheres is known to remove surface impurities, especially sulphur, which reduces adhesion through segregation to the metal–oxide scale interface.

Coating with Y has a similar effect as heat-treating in reducing atmospheres. A combination of a Y-coating and a reducing atmosphere is expected to have the greatest effect on scale adhesion improvement for long oxidation times. Belogolovsky et al. [140] believe that anything that can reduce metal–oxide scale contact area results in poor adhesion and will also increase the ASR of steel interconnects.

Mechanical and thermo-chemical surface treatments can give rise to promising results in terms of reduced ASR. Nonetheless, the Cr poisoning issue is still a problem and has to be overcome by application of effective coatings such as spinels.

8. Alloy developments/modifications

In the past, inexpensive commercial grades such as the AISI-SAE 400 series (e.g., 430, 434, 444, etc.) were the mostly widely utilized steels for SOFC interconnect applications. The ASR of such steels, however, increases rapidly with oxidation and this is attributed to poor scale-to-metal adhesion, segregation of insulating oxides (i.e., silica) at the metal–oxide scale interface and spallation of the scale as a result of interfacial defects combined with thermal stresses. In addition to Si, which may form continuous insulating layers, indigenous impurities such as S can dramatically deteriorate oxide scale-to-metal adhesion as these impurities also accumulate at the metal–oxide scale interface. Spallation of alumina and chromia scales is attributed directly to the presence of trace amounts of S (e.g., ~50 ppm) and its segregation to the metal–oxide scale interface [96,99,105]. On the other hand, the addition of trace amounts of reactive elements (e.g., La, Y, Ce, Hf, Zr, Ti, etc.) to the alloy inhibits interfacial segregation of impurities and greatly enhances oxide scale-to-metal adhesion [97–99]. Furthermore, the presence of even small amounts of Al in the steel composition can lead to internal oxidation and delamination of the oxide scale for long oxidation periods.

To overcome the drawbacks associated with the use of common ferritic stainless steel grades with non-optimal compositions, some specialty alloys have been developed specifically for the purpose of interconnect applications. The reduced amount of impurities, particularly Si and Al, and the addition of reactive elements are the common features of the newly developed alloys. Examples of relatively newly developed ferritic stainless steels include E-brite, Crofer 22 APU, ZMG232 and ZMG232L[1]. All these steels contain lower levels of C, S, P, Mn and Si and higher concentrations of Cr in comparison with the typical formerly used steels.

E-brite[1] (UNS 44627, ASTM Type XM-27), which is manufactured by Allegheny Ludlum, typically contains up to 26 wt.% Cr, 0.05 wt.% Mn, 0.20 wt.% Si, 1 wt.% Mo, 0.02 wt.% Cu, 0.1 wt.% Nb, 0.02 wt.% S (max.), 0.02 wt.% P (max.) and 0.01 wt.% C (max.) [141]. This alloy does not contain any reactive elements. E-brite is highly oxidation resistant; its specific mass gain is 0.4 mg cm^{-2} after 2000 h of cyclic oxidation (twenty 100-h cycles) in air at 800 °C [9]. The ASR for E-brite is approximately 0.015 Ω cm^2 at 800 °C after 250 h of oxidation in air [53].

Crofer 22 APU is a specially designed interconnect alloy commercialized by ThyssenKrupp. This alloy contains 20–24 wt.% Cr, 0.5 wt.% Si, 0.02 wt.% S (max.), 0.05 wt.% P (max.), 0.03 wt.% C, 0.03–0.2 wt.% Ti and 0.04–0.2 wt.% La [142]. In addition to its relatively low levels of impurities, this alloy contains Ti and La as reactive elements. The ASR of Crofer 22 APU is approximately 0.01 Ω cm^2 at 800 °C and remains stable for a test period of 600 h [142]. The specific mass gain of this alloy is 1.25 mg cm^{-2} for cyclic oxidation in air at 800 °C for 2000 h (twenty 100-h cycles) [9].

ZMG232 and its newer, modified adaptation, ZMG232L, have been developed for SOFC interconnect purposes by Hitachi Metals. ZMG232 contains 22 wt.% Cr, 0.4 wt.% Si, 0.02 wt.% C, 0.22 wt.% Zr and 0.03–0.08 wt.% La [143]. Zirconium and La, as reactive elements, are incorporated into the steel composition. ZMG232L has virtually the same composition as ZMG232 except that ZMG232L contains lower levels of Si (i.e., <0.1 wt.%) and Al (<0.04 wt.%). This small Si content difference has a marked effect on oxidation resistance of ZMG232L steels [143]. The specific mass gain obtained with oxidation in air at 750 °C for 2000 h for ZMG232 is 0.5 mg cm^{-2}, while that for ZMG232L is approximately 0.35 mg cm^{-2} [143]. This difference becomes more notable at higher temperatures (2.5 mg cm^{-2} vs. 1 mg cm^{-2} for oxidation at 1000 °C for 100 h) [143]. For both alloys, the level of Si content, however, does not seem to greatly affect the contact resistance. The ASR value for ZMG232 at 750 °C in air after 1000 h was 0.025 Ω cm^2, while that for ZMG232L was approximately 0.022 Ω cm^2 [143]. These values are virtually the same. The ASR for ZMG232 at 800 °C after 1500 h of oxidation was 0.05 Ω cm^2, while that for AISI-SAE 430 was 0.26 Ω cm^2 at 800 °C after 650 h [79]. This difference signifies that by properly adjusting the alloy composition, a marked improvement in the electrical conductivity of the steel interconnects can be achieved.

In a study by Shaigan et al. [16], the metal–oxide scale interface for AISI-SAE 430 and ZMG232 were characterized by means of SEM and surface analysis techniques including secondary ion mass spectroscopy (SIMS), Auger electron analysis (AES) and X-ray photoelectron spectroscopy (XPS). Severe oxide scale spallation occurred for AISI-SAE 430 oxidized at 800 °C in air after less than 100 h, while spallation was not observed for ZMG232 even after longer oxidation times. It was shown that pronounced segregation of Si, S, C, N and other trace impurity elements such as Al, Pb, V, Cl and F occurred at the metal–oxide scale interface for AISI-SAE 430 oxidized at 800 °C. However, for ZMG232, which contains La and Zr as reactive elements, such segregation of impurities was not observed. These elements were, instead, spread throughout the oxide scale in combination with La and Zr. In addition, for AISI-SAE 430, micron-size cavities formed underneath the oxide scale, separating the substrate from the oxide scale. The formation of cavities was attributed to the outward diffusion of Cr during oxidation and the corresponding reduction in the surface energy of void nuclei through impurity segregation, which facilitated the growth of voids and formation of large cavities. Oxide scale spallation for AISI-SAE 430 was attributed to the interfacial defects.

Although marked improvements are achieved with surface treatment, alloy developments and modifications, coatings still seem to be required due to Cr vaporization and Cr poisoning issues, as all the newly developed alloys are chromia formers. A judicious combination of alloy development, surface treatment and coatings can offer a thorough solution to the interconnect problems discussed above. In particular, application of composite, reactive oxide containing spinels on the newly developed alloys (e.g., Crofer 22 APU and ZMG232L) is recommended for future studies.

9. Conclusions

Ferritic stainless steels recently developed specifically for interconnect applications meet the current needs for SOFCs in terms of ASR, CTE match and oxidation resistance for prolonged service times. These alloys commonly contain reactive elements (e.g., La)

to improve the scale adhesion and reduce the oxidation rates. Furthermore, recently developed alloys contain negligible levels of impurities (e.g., Si, Al and S) which helps prevent internal oxidation and scale delamination. Coatings, however, seem to be required, particularly on the cathode side, to prevent Cr transport and cathode Cr poisoning. Among various coatings developed so far, spinels show excellent capability for blocking outward diffusing Cr. Spinels can also be good electronic conductors if the composition is appropriately selected (e.g., $(Co,Mn)_3O_4$, Co_3O_4 and $(Cu,Mn)_3O_4$ show high conductivities). Among the variety of methods developed for application of spinel layers, electrodeposition followed by air annealing offers advantages including the possibility of coating complex interconnect configurations and the formation of uniform, dense and adherent thermally grown spinels. The protection properties of the spinels obtained via electrodeposition can be greatly improved by addition of reactive element oxides to the deposited metallic layer. A combination of an appropriate substrate alloy and coating can fully address issues associated with metallic interconnects.

Acknowledgments

The authors are thankful to the Natural Sciences and Engineering Research Council of Canada (NSERC) and Versa Power Systems (VPS) for providing financial support.

References

[1] W.Z. Zhu, S.C. Deevi, Materials Science and Engineering A-Structural Materials Properties Microstructure and Processing 348 (2003) 227–243.
[2] Z.G. Yang, K.S. Weil, D.M. Paxton, J.W. Stevenson, Journal of the Electrochemical Society 150 (2003) A1188–A1201.
[3] Z.G. Yang, International Materials Reviews 53 (2008) 39–54.
[4] W.J. Quadakkers, J. Piron-Abellan, V. Shemet, L. Singheiser, Materials at High Temperatures 20 (2003) 115–127.
[5] X. Montero, F. Tietz, D. Stover, M. Cassir, I. Villarreal, Corrosion Science 51 (2009) 110–118.
[6] B. Hua, J. Pu, J.F. Zhang, F.S. Lu, B. Chi, L. Jian, Journal of the Electrochemical Society 156 (2009) B93–B98.
[7] Z.G. Yang, G.G. Xia, C.M. Wang, Z.M. Nie, J. Templeton, J.W. Stevenson, P. Singh, Journal of Power Sources 183 (2008) 660–667.
[8] S.J. Geng, J.H. Zhu, M.P. Brady, H.U. Anderson, X.D. Zhou, Z.G. Yang, Journal of Power Sources 172 (2007) 775–781.
[9] S.J. Geng, J.H. Zhu, Journal of Power Sources 160 (2006) 1009–1016.
[10] Z.G. Yang, P. Singh, J.W. Stevenson, G.G. Xia, Journal of the Electrochemical Society 153 (2006) A1873–A1879.
[11] S.J. Geng, J.H. Zhu, Z.G. Lu, Scripta Materialia 55 (2006) 239–242.
[12] J.W. Fergus, Materials Science and Engineering A-Structural Materials Properties Microstructure and Processing 397 (2005) 271–283.
[13] S.P. Simner, M.D. Anderson, G.G. Xia, Z. Yang, L.R. Pederson, J.W. Stevenson, Journal of the Electrochemical Society 152 (2005) A740–A745.
[14] Z.G. Yang, M.S. Walker, P. Singh, J.W. Stevenson, T. Norby, Journal of the Electrochemical Society 151 (2004) B669–B678.
[15] Z.G. Yang, J.S. Hardy, M.S. Walker, G.G. Xia, S.P. Simner, J.W. Stevenson, Journal of the Electrochemical Society 151 (2004) A1825–A1831.
[16] N. Shaigan, D.G. Ivey, W.X. Chen, Journal of the Electrochemical Society 156 (2009) B765–B770.
[17] T. Horita, H. Kshimoto, K. Yamaji, N. Sakai, Y.P. Xiong, M.E. Brito, H. Yokokawa, International Journal of Hydrogen Energy 33 (2008) 3962–3969.
[18] P.D. Jablonski, D.E. Alman, Journal of Power Sources 180 (2008) 433–439.
[19] J. Rufner, P. Gannon, P. White, M. Deibert, S. Teintze, R. Smith, H. Chen, International Journal of Hydrogen Energy 33 (2008) 1392–1398.
[20] X. Sun, W.N. Liu, E. Stephens, M.A. Khaleel, Journal of Power Sources 176 (2008) 167–174.
[21] Z.G. Yang, G.G. Xia, M.S. Walker, C.M. Wang, J.W. Stevenson, P. Singh, International Journal of Hydrogen Energy 32 (2007) 3770–3777.
[22] I. Antepara, I. Villarreal, L.M. Rodriguez-Martinez, N. Lecanda, U. Castro, A. Laresgoiti, Journal of Power Sources 151 (2005) 103–107.
[23] Z.G. Yang, G.G. Xia, P. Singh, J.W. Stevenson, Solid State Ionics 176 (2005) 1495–1503.
[24] M.J. Garcia-Vargas, L. Lelait, V. Kolarik, H. Fietzek, M.D. Juez-Lorenzo, Materials at High Temperatures 22 (2005) 245–251.
[25] L. Cooper, S. Benhaddad, A. Wood, D.G. Ivey, Journal of Power Sources 184 (2008) 220–228.
[26] X.B. Chen, L. Zhang, S.P. Jiang, Journal of the Electrochemical Society 155 (2008) B1093–B1101.
[27] S.P. Jiang, Y.D. Zhen, Solid State Ionics 179 (2008) 1459–1464.
[28] J.W. Fergus, International Journal of Hydrogen Energy 32 (2007) 3664–3671.
[29] E. Konysheva, J. Mertens, H. Penkalla, L. Singheiser, K. Hilpert, Journal of the Electrochemical Society 154 (2007) B1252–B1264.
[30] K. Ogasawara, H. Kameda, Y. Matsuzaki, T. Sakurai, T. Uehara, A. Toji, N. Sakai, K. Yamaji, T. Horita, H. Yokokawa, Journal of the Electrochemical Society 154 (2007) B657–B663.
[31] M. Stanislowski, J. Froitzheim, L. Niewolak, W.J. Quadakkers, K. Hilpert, T. Markus, L. Singheiser, Journal of Power Sources 164 (2007) 578–589.
[32] H. Yokokawa, T. Horita, N. Sakai, K. Yamaji, M.E. Brito, Y.P. Xiong, H. Kishimoto, Solid State Ionics 177 (2006) 3193–3198.
[33] E. Konysheva, H. Penkalla, E. Wessel, J. Mertens, U. Seeling, L. Singheiser, K. Hilpert, Journal of the Electrochemical Society 153 (2006) A765–A773.
[34] S.C. Paulson, V.I. Birss, Journal of the Electrochemical Society 151 (2004) A1961–A1968.
[35] Y. Matsuzaki, I. Yasuda, Journal of the Electrochemical Society 148 (2001) A126–A131.
[36] Y. Matsuzaki, I. Yasuda, Solid State Ionics 132 (2000) 271–278.
[37] M. Stanislowski, E. Wessel, K. Hilpert, T. Markus, L. Singheiser, Journal of the Electrochemical Society 154 (2007) A295–A306.
[38] N. Sakai, T. Horita, K. Yamaji, Y.P. Xiong, H. Kishimoto, M.E. Brito, H. Yokokawa, Solid State Ionics 177 (2006) 1933–1939.
[39] Z.G. Yang, G.G. Xia, P. Singh, J.W. Stevenson, Journal of Power Sources 155 (2006) 246–252.
[40] K. Huang, P.Y. Hou, J.B. Goodenough, Materials Research Bulletin 36 (2001) 81–95.
[41] W. Qu, H. Li, D.G. Ivey, Journal of Power Sources 138 (2004) 162–173.
[42] W. Qu, L. Jian, D.G. Ivey, J.M. Hill, Journal of Power Sources 157 (2006) 335–350.
[43] N. Oishi, T. Namikawa, Y. Yamazaki, Surface & Coatings Technology 132 (2000) 58–64.
[44] D.E. Alman, P.D. Jablonski, International Journal of Hydrogen Energy 32 (2007) 3743–3753.
[45] J.S. Yoon, J. Lee, H.J. Hwang, C.M. Whang, J.W. Moon, D.H. Kim, Journal of Power Sources 181 (2008) 281–286.
[46] J.J. Choi, J.H. Lee, D.S. Park, B.D. Hahn, W.H. Yoon, H.T. Lin, Journal of the American Ceramic Society 90 (2007) 1926–1929.
[47] J.J. Choi, D.S. Park, B.D. Hahn, J. Ryu, W.H. Yoon, Journal of the American Ceramic Society 91 (2008) 2601–2606.
[48] B. Hua, J.F. Zhang, F.S. Lu, Y.H. Kong, J. Pu, J. Li, Acta Metallurgica Sinica 45 (2009) 605–609.
[49] E.A. Lee, J.S. Yoon, H.J. Hwang, J.W. Moon, N.U. Cho, Journal of Ceramic Processing Research 9 (2008) 538–543.
[50] C.J. Fu, K.N. Sun, N.Q. Zhang, D.R. Zhou, Rare Metal Materials and Engineering 35 (2006) 1117–1120.
[51] C. Johnson, R. Gemmen, N. Orlovskaya, Composites Part B-Engineering 35 (2004) 167–172.
[52] Y.J. Yang, T.L. Wen, H.Y. Tu, D.Q. Wang, J.H. Yang, Solid State Ionics 135 (2000) 475–479.
[53] Z.G. Yang, G.G. Xia, G.D. Maupin, J.W. Stevenson, Journal of the Electrochemical Society 153 (2006) A1852–A1858.
[54] N. Orlovskaya, A. Coratolo, C. Johnson, R. Gemmen, Journal of the American Ceramic Society 87 (2004) 1981–1987.
[55] I. Belogolovsky, X.D. Zhou, H. Kurokawa, P.Y. Hou, S. Visco, H.U. Anderson, Journal of the Electrochemical Society 154 (2007) B976–B980.
[56] J.H. Zhu, Y. Zhang, A. Basu, Z.G. Lu, M. Paranthaman, D.F. Lee, E.A. Payzant, Surface & Coatings Technology 177 (2004) 65–72.
[57] C.L. Chu, J.Y. Wang, S.Y. Lee, International Journal of Hydrogen Energy 33 (2008) 2536–2546.
[58] X. Chen, P.Y. Hou, C.P. Jacobson, S.J. Visco, L.C. De Jonghe, Solid State Ionics 176 (2005) 425–433.
[59] Z.G. Yang, G.G. Xia, G.D. Maupin, J.W. Stevenson, Surface & Coatings Technology 201 (2006) 4476–4483.
[60] V.I. Gorokhovsky, P.E. Gannon, M.C. Deibert, R.J. Smith, A. Kayani, M. Kopczyk, D. VanVorous, Z.G. Yang, J.W. Stevenson, S. Visco, C. Jacobson, H. Kurokawa, S.W. Sofie, Journal of the Electrochemical Society 153 (2006) A1886–A1893.
[61] P. Piccardo, P. Gannon, S. Chevalier, M. Viviani, A. Barbucci, G. Caboche, R. Amendola, S. Fontana, Surface & Coatings Technology 202 (2007) 1221–1225.
[62] P. Piccardo, R. Amendola, S. Fontana, S. Chevalier, G. Caboches, P. Gannon, Journal of Applied Electrochemistry 39 (2009) 545–551.
[63] H. Chen, J.A. Lucas, W. Priyantha, M. Kopczyk, R.J. Smith, K. Lund, C. Key, M. Finsterbusch, P.E. Gannon, M. Deibert, V.I. Gorokhovsky, V. Shutthanandan, R. Nachimuthu, Surface & Coatings Technology 202 (2008) 4820–4824.
[64] P. Gannon, M. Deibert, P. White, R. Smith, H. Chen, W. Priyantha, J. Lucas, V. Gorokhousky, International Journal of Hydrogen Energy 33 (2008) 3991–4000.
[65] M.R. Bateni, P. Wei, X.H. Deng, A. Petric, Surface & Coatings Technology 201 (2007) 4677–4684.
[66] J.J. Choi, J. Ryu, B.D. Hahn, W.H. Yoon, B.K. Lee, D.S. Park, Journal of Materials Science 44 (2009) 843–848.
[67] B. Hua, J.A. Pu, W. Gong, J.F. Zhang, F.S. Lu, L. Jian, Journal of Power Sources 185 (2008) 419–422.
[68] C.C. Mardare, H. Asteman, M. Spiegel, A. Savan, A. Ludwig, Applied Surface Science 255 (2008) 1850–1859.
[69] X. Montero, F. Tietz, D. Sebold, H.R. Buchkremer, A. Ringuede, M. Cassir, A. Laresgoiti, I. Villarreal, Journal of Power Sources 184 (2008) 172–179.

[70] X. Montero, N. Jordan, J. Piron-Abellan, F. Tietz, D. Stover, M. Cassir, I. Villarreal, Journal of the Electrochemical Society 156 (2009) B188–B196.
[71] P. Wei, X. Deng, M.R. Bateni, A. Petric, Corrosion 63 (2007) 529–536.
[72] W.F. Wei, W.X. Chen, D.G. Ivey, Journal of Power Sources 186 (2009) 428–434.
[73] J.W. Wu, Y.L. Jiang, C. Johnson, X.B. Liu, Journal of Power Sources 177 (2008) 376–385.
[74] J.W. Wu, C.D. Johnson, Y.L. Jiang, R.S. Gemmen, X.B. Liu, Electrochimica Acta 54 (2008) 793–800.
[75] Z.G. Yang, G.G. Xia, S.P. Simner, J.W. Stevenson, Journal of the Electrochemical Society 152 (2005) A1896–A1901.
[76] Z.G. Yang, G.G. Xia, J.W. Stevenson, Electrochemical and Solid State Letters 8 (2005) A168–A170.
[77] Z.G. Yang, G.G. Xia, X.H. Li, J.W. Stevenson, International Journal of Hydrogen Energy 32 (2007) 3648–3654.
[78] Z.G. Yang, G.G. Xia, Z.M. Nie, J. Templeton, J.W. Stevenson, Electrochemical and Solid State Letters 11 (2008) B140–B143.
[79] X.H. Deng, P. Wei, M.R. Bateni, A. Petric, Journal of Power Sources 160 (2006) 1225–1229.
[80] M.J. Garcia-Vargas, M. Zahid, F. Tietz, A. Aslanides, ECS Transactions 7 (2007) 2399–2405.
[81] J.W. Wu, C.D. Johnson, R.S. Gemmen, X.B. Liu, Journal of Power Sources 189 (2009) 1106–1113.
[82] N. Shaigan, D.G. Ivey, W.X. Chen, Journal of Power Sources 185 (2008) 331–337.
[83] N. Shaigan, D.G. Ivey, W.X. Chen, Journal of Power Sources 183 (2008) 651–659.
[84] N. Shaigan, D.G. Ivey, W.X. Chen, Journal of the Electrochemical Society 155 (2008) D278–D284.
[85] S. Fontana, R. Amendola, S. Chevalier, P. Piccardo, G. Caboche, M. Viviani, R. Molins, M. Sennour, Journal of Power Sources 171 (2007) 652–662.
[86] G. Cabouro, G. Caboche, S. Chevalier, R. Piccardo, Journal of Power Sources 156 (2006) 39–44.
[87] L. Mikkelsen, M. Chen, P.V. Hendriksen, A. Persson, N. Pryds, K. Rodrigo, Surface & Coatings Technology 202 (2007) 1262–1266.
[88] D.P. Lim, D.S. Lim, J.S. Oh, I.W. Lyo, Surface & Coatings Technology 200 (2005) 1248–1251.
[89] D.J. Jan, C.T. Lin, C.F. Ai, Thin Solid Films 516 (2008) 6300–6304.
[90] C. Lee, J. Bae, Thin Solid Films 516 (2008) 6432–6437.
[91] W.F. Wei, W. Chen, D.G. Ivey, Chemistry of Materials 19 (2007) 2816–2822.
[92] X.G. Li, J.W. Lee, B.N. Popov, Journal of Power Sources 187 (2009) 356–362.
[93] K.A. Nielsen, A.R. Dinesen, L. Korcakova, L. Mikkelsen, P.V. Hendriksen, F.W. Poulsen, Fuel Cells 6 (2006) 100–106.
[94] W.F. Wei, W.X. Chen, D.G. Ivey, Chemistry of Materials 20 (2008) 1941–1947.
[95] H.B. Qi, D.G. Lees, Oxidation of Metals 53 (2000) 507–527.
[96] P. Fox, D.G. Lees, G.W. Lorimer, Oxidation of Metals 36 (1991) 491–503.
[97] D.P. Whittle, J. Stringer, Philosophical Transactions of the Royal Society of London Series A-Mathematical Physical and Engineering Sciences 295 (1980) 309–329.
[98] I.M. Allam, D.P. Whittle, J. Stringer, Oxidation of Metals 13 (1979) 381–401.
[99] B.A. Pint, Oxidation of Metals 45 (1996) 1–37.
[100] B.A. Pint, A.J. Garrattreed, L.W. Hobbs, Materials at High Temperatures 13 (1995) 3–16.
[101] P.Y. Hou, J. Stringer, Materials Science and Engineering 87 (1987) 295–302.
[102] P.Y. Hou, Journal of Materials Science Letters 19 (2000) 577–578.
[103] P.Y. Hou, Oxidation of Metals 52 (1999) 337–351.
[104] P.Y. Hou, J. Stringer, Journal of the Electrochemical Society 134 (1987) 1836–1849.
[105] D.G. Lees, Proceedings of the Royal Society of London Series A-Mathematical Physical and Engineering Sciences 459 (2003) 1459–1466.
[106] J.E. Sicre, J.T. Dubois, K.J. Eisentra, R.E. Sievers, Journal of the American Chemical Society 91 (1969) 3476–3481.
[107] K.J. Eisentra, R.E. Sievers, Journal of Inorganic & Nuclear Chemistry 29 (1967) 1931–1936.
[108] K.J. Eisentra, R.E. Sievers, Journal of the American Chemical Society 87 (1965) 5254–5256.
[109] G.Y. Meng, H.Z. Song, Q. Dong, D.K. Peng, Solid State Ionics 175 (2004) 29–34.
[110] G. Garcia, R.I. Merino, V.M. Orera, A. Larrea, J.I. Pena, M.A. Laguna-Bercero, J.A. Pardo, J. Santiso, A. Figueras, Chemical Vapor Deposition 10 (2004) 249–252.
[111] G. Garcia, J. Caro, J. Santiso, J.A. Pardo, A. Figueras, A. Abrutis, Chemical Vapor Deposition 9 (2003) 279–284.
[112] H.Z. Song, H.B. Wang, S.W. Zha, D.K. Peng, G.Y. Meng, Solid State Ionics 156 (2003) 249–254.
[113] G. Di Giuseppe, J.R. Selman, Journal of Materials Research 16 (2001) 2983–2991.
[114] H.B. Wang, H.Z. Song, C.R. Xia, D.K. Peng, G.Y. Meng, Materials Research Bulletin 35 (2000) 2363–2370.
[115] G.L. Bertrand, G. Caboche, L.C. Dufour, Solid State Ionics 129 (2000) 219–235.
[116] K.W. Chour, J. Chen, R. Xu, Thin Solid Films 304 (1997) 106–112.
[117] S.L. Rohde, in: C.M. Cotell, J.A. Sprauge, F.A. Smidt Jr. (Eds.), ASM Handbook, ASM International, Materials Park, OH, 1994, pp. 573–581.
[118] J.S. Horwitz, in: C.M. Cotell, J.A. Sprauge, F.A. Smidt Jr. (Eds.), ASM Handbook, ASM International, Materials Park, OH, 1994, pp. 621–626.
[119] W. Qu, L. Jian, J.M. Hill, D.G. Ivey, Journal of Power Sources 153 (2006) 114–124.
[120] A. Petric, H. Ling, Journal of the American Ceramic Society 90 (2007) 1515–1520.
[121] L.A. Chick, L.R. Pederson, G.D. Maupin, J.L. Bates, L.E. Thomas, G.J. Exarhos, Materials Letters 10 (1990) 6–12.
[122] H. Kurokawa, C.P. Jacobson, L.C. DeJonghe, S.J. Visco, Solid State Ionics 178 (2007) 287–296.
[123] D.H. Prasad, H.R. Kim, J.W. Son, B.K. Kim, H.W. Lee, J.H. Lee, Catalysis Communications 10 (2009) 1334–1338.
[124] B. Lin, W.P. Sun, K. Xie, Y.C. Dong, D.H. Dong, X.Q. Liu, J.F. Gao, G.Y. Meng, Journal of Alloys and Compounds 465 (2008) 285–290.
[125] D. Lee, J.H. Han, E.G. Kim, R.H. Song, D.R. Shin, Journal of Power Sources 185 (2008) 207–211.
[126] X.F. Guan, H.P. Zhou, Y. Wang, J. Zhang, Journal of Alloys and Compounds 464 (2008) 310–316.
[127] L.P. Sun, Q. Li, H. Zhao, L.H. Huo, J.C. Grenier, Journal of Power Sources 183 (2008) 43–48.
[128] Y.J. Leng, S.H. Chan, Q.L. Liu, International Journal of Hydrogen Energy 33 (2008) 3808–3817.
[129] Q.G. Wang, R.R. Peng, C.R. Xia, W. Zhu, H.T. Wang, Ceramics International 34 (2008) 1773–1778.
[130] C. Jin, J. Liu, Y.H. Zhang, J. Sui, W.M. Guo, Journal of Power Sources 182 (2008) 482–488.
[131] E.Q. He, W.H. Ma, J. Yu, R.H. Liu, Y.N. Dai, Journal of Rare Earths 25 (2007) 382–386.
[132] X.F. Guan, H.P. Zhou, Z.H. Liu, Y.A. Wang, J. Zhang, Materials Research Bulletin 43 (2008) 1046–1054.
[133] B.W. Liu, Y. Zhang, Journal of Alloys and Compounds 453 (2008) 418–422.
[134] W.I. Zhou, Z.P. Shao, R. Ran, H.X. Gu, W.Q. Jin, N.P. Xu, Journal of the American Ceramic Society 91 (2008) 1155–1162.
[135] R.C. Tucker, in: C.M. Cotell, J.A. Sprauge, F.A. Smidt Jr. (Eds.), ASM Handbook, ASM International, Materials Park, OH, 1994, pp. 497–509.
[136] W.F. Wei, W.X. Chen, D.G. Ivey, Journal of Physical Chemistry C 111 (2007) 10398–10403.
[137] D.M. Sanders, J.W. Glaser, S. Falabelal, in: C.M. Cotell, J.A. Sprauge, F.A. Smidt Jr. (Eds.), ASM Handbook, ASM International, Materials Park, OH, 1994, pp. 602–604.
[138] A. Brenner, Electrodeposition of Alloys Principles and Practice, Academic Press, New York and London, 1963, pp. 137–156.
[139] C. Ostwald, H.J. Grabke, Corrosion Science 46 (2004) 1113–1127.
[140] I. Belogolovsky, P.Y. Hou, C.P. Jacobson, S.J. Visco, Journal of Power Sources 182 (2008) 259–264.
[141] E-Brite Technical Data Blue Sheet, http://www.alleghenytechnologies.com/ludlum/Documents/E-BRITE%20050207.pdf, Allegheny Ludlum, 2007.
[142] Crofer 22 APU Material Data Sheet No. 4046, http://www.thyssenkrupp-vdm-fareast.com/media/down_datasheets_heatres_new/crofer22apu_e.pdf, ThyssenKrupp VDM GmbH, 2005.
[143] A. Toji, T. Uehara, ECS Transactions 7 (2007) 2117–2124.